Impact of interfacial dipole on carrier transport in bulk heterojunction poly„3-hexylthiophene and †6,6‡-phenyl C61-butyric acid methyl ester blends

Tsang, S. W.; Drolet, N.; Tse, S. C.; Tao, Y.; Lu, Z. H.

Publisher's version / Version de l'éditeur:
https://doi.org/10.1063/1.3499368
Applied Physics Letters, 97, 153306, pp. 1-3, 2010-10-14

Impact of interfacial dipole on carrier transport in bulk heterojunction poly(3-hexylthiophene) and [6,6]-phenyl C_{61}-butyric acid methyl ester blends

S. W. Tsang,[1,2,a)] N. Drolet,[2] S. C. Tse,[2] Y. Tao,[2] and Z. H. Lu[1,b)]
[1]*Department of Material Science and Engineering, University of Toronto, Toronto, Ontario M5S 3E4, Canada*
[2]*Institute for Microstructural Sciences, National Research Council of Canada, Ottawa, Ontario K1A 0R6, Canada*

(Received 21 August 2010; accepted 20 September 2010; published online 14 October 2010)

The electron transport properties in various poly(3-hexylthiophene) (P3HT) and [6,6]-phenyl C_{61}-butyric acid methyl ester ($PC_{61}BM$) blend films, prepared by various process conditions, were investigated by admittance spectroscopy at different temperatures. It was found that the electron mobility and the dispersive transport behavior showed a strong dependence on the thermal treatment condition; the blend with the fastest growth rate had orders of magnitude reduction in the mobility and a much more dispersive transport. Using the Gaussian disorder model, it was found that the energetic disorder of the density-of-states between blends plays a significant role in the observed phenomena. It is proposed that the difference in the energetic disorder is due to the interfacial dipole effect at the P3HT/$PC_{61}BM$ heterojunctions in the various blend films. © *2010 American Institute of Physics*. [doi:10.1063/1.3499368]

It is well-known that the efficiency of the bulk-heterojunction organic photovoltaics cells (OPVs) is highly sensitive to the nanoscale morphology of the active layer.[1–5] It is mainly determined by the growth rate of the active layer right after spin-casting. The electron donor poly(3-hexylthiophene) (P3HT) and the electron acceptor [6,6]-phenyl C_{61}-butyric acid methyl ester ($PC_{61}BM$) are prototypical materials in OPV technology. It has been demonstrated that the power conversion efficiency (PCE) for P3HT:$PC_{61}BM$ device can be varied from 3–6% with different growth conditions of the polymer blend. Such variations in device performance is closely related to the balance between the exciton diffusion and the carrier transport with different domain sizes of the donor and acceptor materials. It is generally believed that the degree of ordering of the active material, the spatial effect, is necessarily the key factor in determining the charge-carrier transport properties.[6] However, recently, it has been observed that a spontaneous transfer of a negative charge from P3HT:PC_{60} in bilayer structure forms an interface dipole.[7] Similarly, in P3HT:$PC_{61}BM$ bulk-heterojunctions, there are numerous interfaces between the individual materials. It can be deduced that the presence of the possible dipoles at these numerous interfaces will alter the charge-carrier transport properties in the blend film.

In this letter, the authors report on the electron transport properties in various P3HT:$PC_{61}BM$ blends as a function of the film microstructure. Admittance spectroscopy (AS), a powerful tool for probing the charge carrier dynamics, is employed to extract the electron mobility at various temperatures and to understand the physical mechanism for electron transport in the bulk-heterojunction thin films.

The samples fabricated in this study consist of a single active layer of P3HT:$PC_{61}BM$ (1:1, wt %) sandwiched between an anode (Al, 70 nm) and a cathode (Mg:Ag, 10:1, 50 nm) on glass substrates. The cathode was further covered by 50 nm of Ag used as capping layer. The metal electrodes were thermally evaporated in vacuum at a base pressure of 10^{-7} Torr. The active layers were prepared by spin-coating the blend solution in dichlorobenzene onto the Al electrode. The organization in the active layer was controlled by varying the growth rate of the active layer. Control of the growth rate was achieved by controlling the solution concentration, spinning speed and thermal treatment of the active layer after spin-coating. Details of the active layer preparation conditions are summarized in Table I. The growth rate in the different samples was in the order of sample A > B > C > D. The thicknesses of the active layer were measured by a profilometer. The electron mobility in P3HT:$PC_{61}BM$ thin films was characterized by AS with an HP 4284A LRC meter. Details of the principle and the experiment setup of AS have been reported elsewhere.[8] Although electron injection from Mg:Ag into P3HT is possible, the injected electrons will be rapidly transferred to the $PC_{61}BM$ molecules which has a lower lowest-unoccupied molecular orbital energy level. Prior to the charge carrier mobility measurements, any absorbed ambient effect during sample transfer or residual solvent was eliminated by moderately heating the sample at 50 °C for 24 h inside a temperature regulated cryostat with a base pressure of 10^{-6} Torr.

Figure 1 shows the typical capacitance versus frequency characteristics of the different samples measured by AS. A

TABLE I. Summary of preparation condition of the P3HT:$PC_{61}BM$ (1:1, wt %) blends.

Sample	Solution concentration (mg/ml)	Spinning condition (rpm)	Thermal treatment	Thickness (μm)
A	112	1000 (60s)	Baked 200 °C (30mins)	1.20
B	112	1000 (60s)	Baked 100 °C (30mins)	1.16
C	112	1000 (60s)	Naturally dried for 24 h	1.16
D	42.5	300 (60s)	Naturally dried for 24 h	1.50

a)Author whom correspondence should be addressed. Electronic mail: saiwing.tsang@nrc-cnrc.gc.ca.
b)Electronic mail: zhenghong.lu@utoronto.ca.

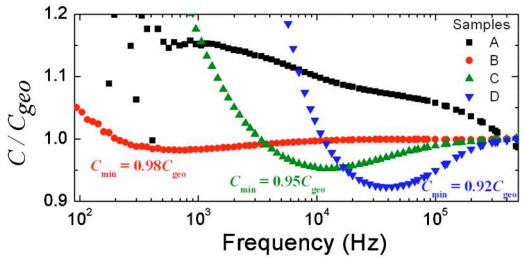

FIG. 1. (Color online) Measured capacitance vs frequency characteristics of sample A (black, square) at $T=263$ K and $F=2.0\times10^5$ V/cm; B (red, circle) at $T=263$ K and $F=2.0\times10^5$ V/cm; C (green, up-triangle) at $T=263$ K and $F=2.0\times10^5$ V/cm; D (blue, down-triangle) at $T=270$ K and $F=1.3\times10^4$ V/cm. The capacitance C is normalized to the geometrical capacitance C_{geo} of individual sample.

minimum capacitance C_{min} at a certain frequency is found in samples B, C, and D. This feature corresponds to the space charge effect in the bulk of the material.[8,9] It also proves that a quasi-Ohmic contact is formed at the Mg:Ag/$PC_{61}BM$ interface.[10] The electron mobility μ_e can be effectively extracted from the measured capacitance. Briefly, if C_{min} occurs at higher frequency it indicates a higher charge carrier mobility. Therefore, μ_e increases from sample B to sample D, corresponding to a fast and a slow growth rate, respectively. Moreover, the degree of charge carrier mobility dispersion can be revealed by considering the ratio of C_{min}/C_{geo}, where C_{geo} is the geometrical capacitance of the sample. In the case of nondispersive transport, $C_{min}/C_{geo}=0.75$.[8,9] The value of C_{min}/C_{geo} increases for more dispersive transport. For highly dispersive transport the capacitance minimum vanishes. As shown in Fig. 1, there is no capacitance minimum observed in sample A. The value of C_{min}/C_{geo} decreases from 0.98 in sample B to 0.92 in sample D, which suggests that the electron transport becomes less dispersive as the growth rate of the active layer decreases. It is worth considering that the dispersive transport behavior can originate from the presence of trap states, or from the disordered properties of the transporting sites, both positional and energetic. However, since the samples are prepared with the same batch of materials, the variation in bulk trap states in different samples is safely excluded. Furthermore, it has been demonstrated that a slower growth rate of the active layer leads to a more ordered P3HT:$PC_{61}BM$ film.[3,5] Therefore, the difference of the disordered properties between samples is attributed to the variation in the observed electron transport behavior.

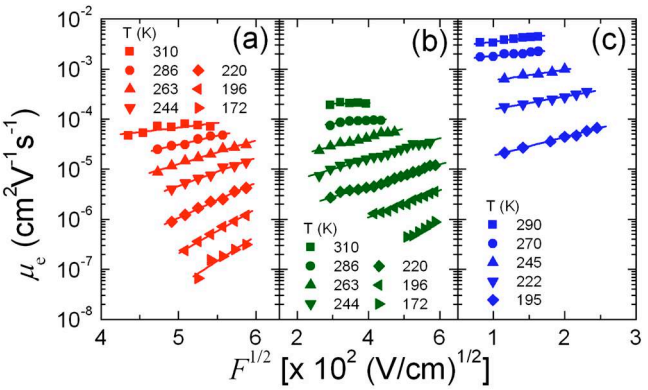

FIG. 2. (Color online) Measured electron mobility μ_e vs square root of applied electric field $F^{1/2}$ of sample (a) B (red), (b) C (green), and (c) D (blue). The solid lines are the best fit of the data to the Pool–Frenkel type of electric field F dependence $\mu_e \propto \exp(\beta F^{1/2})$.

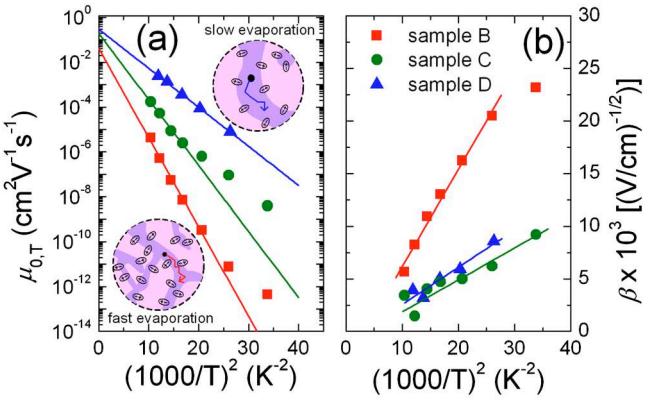

FIG. 3. (Color online) (a) The zero-field mobility $\mu_{0,T}$ extrapolated from the measured μ_e in Fig. 2 vs $1/T^2$ of sample B (red), C (green), and D (blue). (b) The corresponding field dependence coefficient β vs $1/T^2$. The solid lines are the best fits to the data at temperature $T>220$ K. Insets show the illustrations of the phase segregation of P3HT:$PC_{61}BM$ for slow and fast growth rate of the active layer. Interface dipoles are formed at P3HT:$PC_{61}BM$ heterojunctions.

The electron mobilities of sample B, C, and D measured by AS at various temperatures are shown in Fig. 2. In general, the mobilities follow the Poole–Frenkel type of electric field F dependence $\mu_e \propto \exp(\beta F^{1/2})$, where β is the field dependence coefficient. It is found that μ_e in sample B, which has the fastest growth rate among samples B, C, and D, has the highest temperature and electric field dependence. From the measured μ_e, the disordered properties of the electron transporting site in $PC_{61}BM$ can be revealed by analyzing the data with the Gaussian disordered model (GDM):[11]

$$\mu(E,T) = \mu_{inf} \exp\left[-\left(\frac{2\sigma}{3kT}\right)^2\right] \exp\left\{C\left[\left(\frac{\sigma}{kT}\right)^2 - \Sigma^2\right]\sqrt{F}\right\}, \quad (1)$$

where μ_{inf} is a prefactor, σ is the energetic disorder parameter that can be understood as the width of the Gaussian density-of-state (DOS), Σ is the positional disorder parameter, and C is a constant. By extrapolating the measured μ_e to zero field, σ can be obtained from the plot of the zero field mobility $\mu_{0,T}$ versus $1/T^2$ as shown in Fig. 3(a). On the other hand, Σ can be extracted by plotting β versus $1/T^2$ as shown in Fig. 3(b). The extracted disorder parameters for different samples are summarized in Table II. As expected, the largest positional disorder parameter Σ is found in sample B and the smallest in sample D. A more organized film of P3HT:$PC_{61}BM$ blend can be formed from a slower growth rate of the active layer. Although it is generally believed that such improved ordering is only a result of the increase in crystalline packing of P3HT, there is no doubt that more $PC_{61}BM$ will also pack together to retain a constant effective volume. This has been proved by the observed phase segregation between P3HT and $PC_{61}BM$ measured by atomic force microscopy.[4] Surprisingly, there is a large difference in

TABLE II. Extracted GDM parameters of different samples from the measured electron mobility μ_e in Fig. 3.

Sample	μ_{inf} (cm^2 V^{-1} s^{-1})	σ (meV)	C (V/cm)$^{-1}$	Σ
B	0.041	124	4.53×10^{-4}	2.63
C	0.19	106	2.12×10^{-4}	2.06
D	0.30	82	3.93×10^{-4}	1.58

the energetic disorder parameter σ between different samples. As depicted in Eq. (1), the low field mobility is mainly determined by the μ_{inf} and σ. Taking sample B and D as an example, μ_{inf} in sample B is about one order of magnitude lower than that in sample D. However, a large value of σ in sample B attributes to more than two orders of magnitude reduction in mobility. Extensive experimental studies on carrier transport properties in polymers doped with hole-transporting molecules have been reported by Borsenberger and co-workers,[12,13] with detailed discussion of μ_{inf} and σ in different polymer hosts. The prefactor μ_{inf} depends on the intersite distance R and wave function decay constant α, i.e., $\mu_{inf} \propto R^2 \exp(-2\alpha R)$. Owning to the energy difference of the transporting sites in P3HT and $PC_{61}BM$, the wave function overlap is larger between $PC_{61}BM$ molecules. Moreover, in a less organized blend that with smaller degree of phase segregation, more $PC_{61}BM$ molecules are homogeneously dispersed with the P3HT polymers which increases the intermolecular distance R between the $PC_{61}BM$ molecules for electron transport. Considering a typical value of $\alpha = 5 \times 10^7$ cm^{-1} for organic materials,[14,15] and R varies from a few to tens of nanometers which depends on the processing conditions. A larger R in the less organized blend reduces the μ_{inf}. Despite the spatial effect, it is found that the increased energetic disorder of $PC_{61}BM$ in the less organized blend also plays an important role for the reduction in the electron mobility.

The variation in σ in different blend films can be explained by considering the presence of interface dipoles between P3HT and $PC_{61}BM$. The dipolar effect on the energy profile of the DOS and the charge-carrier transport in a disordered media was originally proposed by Dieckmann[16] and Young[17] under the framework of the GDM. The energetic disorder parameter takes into account both the dipole-induced disorder σ_d and the Van der Waals interactions between molecules σ_{vdw}, i.e., $\sigma^2 = \sigma_d^2 + \sigma_{vdw}^2$. The additional σ_d broadens the Gaussian DOS which depends on the amount and the orientation of the dipole moments in the system.[17] It has been recently reported that there exists an interface dipole between P3HT and C_{60} by photoemission study.[7] Assuming the magnitude of the dipole at the P3HT/$PC_{61}BM$ interface in different blend films are comparable, it is proposed that the origin of the difference of σ_d between samples with slower and faster growth rate of the active layer is due to the variation of the interfacial area of the heterojunctions as illustrated in the insets of Fig. 3(a). Less phase segregation between P3HT and $PC_{61}BM$ is expected for the film grown faster. The area of the P3HT/$PC_{61}BM$ interface, and therefore the number of interface dipoles is larger inside this blend. Moreover, as the $PC_{61}BM$ phase is smaller, the injected electrons have higher probability to experience the interface dipole effect during the multidirectional hopping process. This attributes to a larger overall energetic disorder σ for the sample having a faster growth rate of the active layer. A larger σ reduces the electron mobility and results in much more dispersive transport behavior. In other words, in the absence of dipoles at the P3HT/$PC_{61}BM$ interface, the difference in charge carrier mobility between samples are mainly determined by the prefactor μ_{inf} and the positional disorder parameter Σ, which depends on the degree of the self-organization of samples. However, the presence of dipoles at the P3HT/$PC_{61}BM$ interface additionally increases the energetic disorder parameter σ which further reduces the charge carrier mobility. The contribution of the dipole disorder σ_d also depends on the degree of the self-organization of the samples; a larger σ_d is expected in less organized blends that have larger P3HT/$PC_{61}BM$ interface area.

In conclusion, the electron transport properties in P3HT:$PC_{61}BM$ (1:1) blend films have been studied by AS at various temperatures. It is found that both the electron mobility and the dispersive transport behavior depend strongly on the growth rate of the active layer. According to the results of the measured electron mobility of different samples at various temperatures, the electron mobility is mainly determined by the variation in the energetic disorder, rather than by the spatial distribution of the transporting sites in $PC_{61}BM$. This is proposed to be a result of the variation in the induced-dipole disorder at the P3HT/$PC_{61}BM$ interfaces within the blend films. A faster growth rate with less phase segregation between P3HT and $PC_{61}BM$ leads to larger effective area of interfacial dipole at the P3HT/$PC_{61}BM$ heterojunctions which impede electron transport in the blend films by increasing the energetic disorder of the DOS.

Financial support for this project was provided by Natural Sciences and Engineering Research Council of Canada (NSERC) and National Research Council Canada (NRC).

[1] W. Ma, C. Yang, X. Gong, K. H. Lee, and A. J. Heeger, Adv. Funct. Mater. **15**, 1617 (2005).
[2] G. Li, V. Shrotriya, J. Huang, Y. Yao, T. Moriarty, K. Emery, and Y. Yang, Nature Mater. **4**, 864 (2005).
[3] Y. Kim, S. Cook, S. M. Tuladhar, S. A. Choulis, J. Nelson, J. R. Durrant, D. D. C. Bradley, M. Giles, I. McCulloch, C.-S. Ha, and M. Ree, Nature Mater. **5**, 197 (2006).
[4] V. Shrotriya, Y. Yao, G. Li, and Y. Yang, Appl. Phys. Lett. **89**, 063505 (2006).
[5] C.-W. Chu, H. Yang, W.-J. Hou, J. Huang, G. Li, and Y. Yang, Appl. Phys. Lett. **92**, 103306 (2008).
[6] R. Pacios, J. Nelson, D. D. C. Bradley, and C. J. Brabec, Appl. Phys. Lett. **83**, 4764 (2003); S. A. Choulis, J. Nelson, Y. Kim, D. Poplavskyy, T. Kreouzis, J. R. Durrant, and D. D. C. Bradley, Appl. Phys. Lett. **83**, 3812 (2003); J. Huang, G. Li, and Y. Yang, Appl. Phys. Lett. **87**, 112105 (2005).
[7] W. Osikowicz, M. P. Jong, and W. R. Salaneck, Adv. Mater. **19**, 4213 (2007).
[8] S. W. Tsang, S. K. So, and J. B. Xu, J. Appl. Phys. **99**, 013706 (2006).
[9] H. C. F. Martens, H. B. Brom, and P. W. M. Blom, Phys. Rev. B **60**, R8489 (1999).
[10] S. W. Tsang, S. C. Tse, K. L. Tong, and S. K. So, Org. Electron. **7**, 474 (2006).
[11] H. Bässler, Phys. Status Solidi B **175**, 15 (1993).
[12] P. M. Borsenberger, J. Appl. Phys. **68**, 5188 (1990).
[13] J. A. Sinicropi, J. R. Cowdery-Corvan, E. H. Magin, and P. M. Borsenberger, Proc. SPIE **2850**, 202 (1996).
[14] E. L. Wolf, *Principle of Electron Tunneling Spectroscopy* (Oxford University Press, New York, 1995).
[15] S. W. Tsang, M. W. Denhoff, Y. Tao, and Z. H. Lu, Phys. Rev. B **78**, 081301(R) (2008).
[16] A. Dieckmann, H. Bässler, and P. M. Borsenberger, J. Chem. Phys. **99**, 8136 (1993).
[17] R. H. Young, Philos. Mag. B **72**, 435 (1995).